Journal of Magnetic Resonance 361 (2024) 107629

Contents lists available at ScienceDirect

Journal of Magnetic Resonance

journal homepage: www.elsevier.com/locate/jmr

Optimization of TROSY- and anti-TROSY-based ^{15}N CPMG relaxation dispersion experiments through phase cycling

Yingxian Cui [a,1], Yangzhuoyue Jin [a,1], Yu Hou [a], Xiaoxu Han [a], Haiyan Cao [a], Lewis E. Kay [b,c,d,e,*], Tairan Yuwen [a,*]

[a] State Key Laboratory of Natural and Biomimetic Drugs, Department of Pharmaceutical Analysis, School of Pharmaceutical Sciences, Peking University, Beijing 100191, China
[b] Department of Molecular Genetics, University of Toronto, Toronto, Ontario M5S 1A8, Canada
[c] Department of Biochemistry, University of Toronto, Toronto, Ontario M5S 1A8, Canada
[d] Department of Chemistry, University of Toronto, Toronto, Ontario M5S 3H6, Canada
[e] Program in Molecular Medicine, Hospital for Sick Children Research Institute, Toronto, Ontario M5G 1X8, Canada

ARTICLE INFO

Keywords:
Protein dynamics
Chemical exchange
CPMG
Invisible excited states
TROSY
Phase cycle

ABSTRACT

CPMG relaxation dispersion studies of biomolecular dynamics on the μs–ms timescale can provide detailed kinetic, thermodynamic, and structural insights into function. Frequently, the ^{15}N spin serves as the probe of choice, as uniform incorporation of the ^{15}N isotope is facile and cost-effective, and the interpretation of the resulting data is often relatively straightforward. In conventional CPMG relaxation dispersion experiments the application of CPMG pulses with constant radiofrequency (RF) phase can lead to artifactual dispersion profiles that result from off-resonance effects, RF field inhomogeneity, and pulse miscalibration. The development of CPMG experiments with the [0013]-phase cycle has significantly reduced the impact of pulse imperfections over a greater bandwidth of frequency offsets in comparison to constant phase experiments. Application of ^{15}N-TROSY-based CPMG schemes to studies of the dynamics of large molecules is necessary for high sensitivity, yet the correct incorporation of the [0013]-phase cycle is non-trivial. Here we present TROSY- and anti-TROSY-based ^{15}N CPMG experiments with the [0013]-phase cycling scheme and demonstrate, through comprehensive numerical simulations and experimental validation, enhanced resistance to pulse imperfections relative to traditional schemes utilizing constant phase CPMG pulses. Notably, exchange parameters derived from the new experiments are in good agreement with those obtained using other, more established, ^{15}N-based CPMG approaches.

1. Introduction

The dynamic behavior of biomolecules spans a diverse range of timescales, the consequence of complex free energy landscapes involving multitudes of interactions. These dynamics can be critical for function [1–4] and misfunction [5–7] and have been the focus of a large number of studies using a variety of different methodologies. NMR spectroscopy is one of the most powerful tools for probing molecular dynamics, with diverse NMR experiments tailored to study motion across a wide window of time scales [8], including the microsecond to millisecond (μs–ms) range [9] for which a variety of experiments have been designed. These include Carr–Purcell–Meiboom–Gill (CPMG) relaxation dispersion [10,11], Chemical Exchange Saturation Transfer (CEST) [12,13], $R_{1\rho}$ relaxation dispersion [14,15], and Dark State Exchange Transfer (DEST) [16] approaches.

CPMG relaxation dispersion is perhaps the most popular technique for providing insight into otherwise "invisible" excited states of biomolecules [17]. Here, the apparent transverse relaxation rates ($R_{2,eff}$) of observable spins are modulated through the application of CPMG pulses at a frequency $\nu_{CPMG} = 1/(4\tau_{cp})$, where $2\tau_{cp}$ is the delay between consecutive pulses in a pulse train. Fits of an appropriate exchange model to the obtained $R_{2,eff}$ profiles as a function of ν_{CPMG} enable the extraction of kinetic and thermodynamic parameters and, potentially, a wealth of information about the rare conformationally excited state(s) exchanging with the ground state, including but not limited to chemical shifts (ϖ_E), residual dipolar couplings (RDCs) [18], ps–ns relaxation parameters [19], hydrogen exchange rates [20], pseudocontact shifts (PCS) [21,22], and diffusion constants [23].

The extraction of robust chemical exchange parameters is predicated on artifact free CPMG pulse trains that can consist of a hundred

* Corresponding authors.
E-mail addresses: lewis.kay@utoronto.ca (L.E. Kay), tyuwen@pku.edu.cn (T. Yuwen).
[1] These authors contributed equally.

https://doi.org/10.1016/j.jmr.2024.107629
Received 4 January 2024; Revised 26 January 2024; Accepted 27 January 2024
Available online 2 February 2024

pulses or more. Unless special precautions are taken errors can accumulate, leading to artifacts in dispersion profiles and concomitant reduction in the quality of the obtained dynamics information. To this end composite [23–28] or shaped [29–31] pulses have been used, along with phase cycling schemes to refocus artifacts. Of particular note to the work presented here, Yip and Zuiderweg have described the integration of a [0013]-phase cycle [32] within CPMG pulse trains that very significantly mitigates artifacts arising from pulse imperfections. Building on this important advance Yang and coworkers presented an improved ^{15}N single quantum experiment, referred to as ^{15}N ST-CW-CPMG in what follows [33], that exhibits superior performance compared to most other counterparts [34,35].

It is anticipated that the benefits of the [0013]-phase cycle would extend well beyond simple ^{15}N single quantum CPMG experiments, to include TROSY-based CPMG measurements [36], which are particularly well-suited for investigating dynamics in large biomolecules [37]. However, care must be taken in the incorporation of [0013]-phase cycles in TROSY sequences due to the requisite S^{3}CT selective inversion element (or P element) in the middle of the CPMG pulse train in this case [37]. To the best of our knowledge no such experiment has yet been proposed. Herein, we present TROSY- and anti-TROSY-based ^{15}N CPMG pulse schemes that include [0013]-phase cycles of pulse elements in the CPMG trains, referred to as [0013]-TROSY and [0013]-anti-TROSY CPMG, respectively, and provide a detailed theoretical description of how such a phase cycle can be incorporated. We demonstrate, both theoretically and experimentally, improved performance with respect to pulse imperfections relative to experiments with constant phase CPMG pulses and present applications to a number of protein systems. The [0013]-modification further strengthens the ^{15}N CPMG-TROSY experiment [18,37] as a valuable tool for probing μs–ms dynamics in high molecular weight biomolecules, as well as the ^{15}N TROSY/anti-TROSY CPMG pair that is used for the measurement of RDCs in excited protein states [18].

2. Materials and methods

2.1. Sample preparation

The B1 domain of peptostreptococcal protein L, denoted as protein L hereafter, was prepared in accordance with established protocols [38,39]. A 4.0 mM sample of U-[^{15}N,^{2}H]-labeled protein was generated in a buffer comprising 50 mM sodium phosphate, 0.05 % NaN_3, 90 % H_2O/10 % D_2O, and pH 6.0. The NMR sample of U-[^{15}N,^{2}H] G48A FynSH3 was prepared as described previously [40]. The protein concentration for this sample was 1.35 mM, dissolved in a buffer consisting of 50 mM sodium phosphate, 0.2 mM EDTA, 0.05 % NaN_3, 90 % H_2O/10 % D_2O, and pH 7.0. A U-[^{15}N,^{2}H] L99A T4 lysozyme sample, designated as L99A T4L henceforth, was generated according to Bouvignies et al. [41]. The sample concentration for L99A T4L was 1.5 mM, dissolved in a buffer of 50 mM sodium phosphate, 25 mM NaCl, 2 mM EDTA, 2 mM NaN_3, 90 % H_2O/10 % D_2O, and pH 5.5.

2.2. NMR spectroscopy

NMR experiments were conducted on Bruker 800 MHz and 600 MHz spectrometers equipped with z-axis cryogenically cooled probes. Sample temperatures were 4 °C for protein L and 25 °C for G48A FynSH3 and L99A T4L. In addition to recording ^{15}N CPMG dispersion experiments using the pulse schemes proposed here, we also recorded corresponding datasets using the ^{15}N ST-CW-CPMG experiment of Yang and coworkers [33], along with previously developed TROSY- and anti-TROSY-based ^{15}N CPMG experiments [18]. Pseudo-3D datasets were recorded by varying the number of CPMG pulses ($2N$) during a constant-time relaxation delay (T_{relax}) [42] in each 2D plane. For protein L (both TROSY and anti-TROSY experiments) and L99A T4L (anti-TROSY experiments), T_{relax} = 30 ms, while for G48A FynSH3 (both TROSY and anti-TROSY experiments) and L99A T4L (TROSY experiments), T_{relax} = 40 ms; the choice of T_{relax} was guided by ensuring that peak intensities decay to approximately 50 % relative to the reference spectrum without the T_{relax} period. CPMG pulse frequencies (ν_{CPMG}) spanning 33 to 1000 Hz were applied for protein L (TROSY and anti-TROSY) and L99A T4L (anti-TROSY), and 25 to 1000 Hz for G48A FynSH3 (TROSY and anti-TROSY) and L99A T4L (TROSY). For the ^{15}N ST-CW-CPMG scheme a ^{1}H continuous wave (CW) field strength of approximately 15 kHz was applied during the T_{relax} delay. A pre-scan delay of 2.0 s was utilized for recording all datasets and the S^{3}E element was applied in all TROSY-/anti-TROSY-based CPMG experiments using both the [0013]-phase cycle and the constant phase CPMG pulse trains, unless otherwise specified.

2.3. Data analysis

All NMR datasets are processed and analyzed using the *NMRPipe* suite of programs [43], with peak intensities extracted utilizing the *autofit* subroutine. The effective transverse relaxation rate, $R_{2,eff}$, for each CPMG pulse frequency (ν_{CPMG}) is determined via $R_{2,eff}(\nu_{CPMG}) = -\ln(I(\nu_{CPMG})/I_0)/T_{relax}$, where I_0 is the peak intensity in a reference spectrum recorded without the T_{relax} period [42]. Fits of $R_{2,eff}(\nu_{CPMG})$ were carried out using the *ChemEx* software package [44], using a two-state exchange model, $G \underset{k_{EG}}{\overset{k_{GE}}{\rightleftarrows}} E$. Values of ($p_E$, k_{ex}), where p_E is the fractional population of the excited conformational state and $k_{ex} = k_{GE} + k_{EG}$, are derived as global parameters through the analysis of CPMG datasets measured on both 600 MHz and 800 MHz spectrometers. In addition, values of $|\Delta\varpi_{GE}| = |\varpi_E - \varpi_G|$, where ϖ_I is the ^{15}N chemical shift (ppm) of each residue in state I, were obtained from the analysis. The root-mean-square deviation (RMSD) of each relaxation dispersion profile to a horizontal best fit line is defined as $RMSD = \sqrt{\frac{1}{N}\sum_{i=1}^{N}\left(R_{2,eff}^{i} - R_{2,eff}^{avg}\right)^2}$, where i is the index of a particular ν_{CPMG} value and $R_{2,eff}^{avg}$ is the average of $R_{2,eff}$ over the N points within the profile. The numerical fitting module and example datasets are available from the GitHub repository of *ChemEx* [44].

2.4. Numerical simulations

All numerical simulations evaluating the performance of a variety of CPMG pulse trains were carried out using home-written Python programs (only the CPMG relaxation dispersion period within a given pulse sequence was simulated). The evolution of the spin density matrix (ρ) during the CPMG relaxation dispersion pulse train was computed using the Liouville-von Neumann equation, incorporating relaxation and chemical exchange effects as outlined in previous studies [45,46]. The initial density matrix, $\rho(t = 0)$, was S_yI^{β} or S_yI^{α} (for TROSY or anti-TROSY schemes, respectively, when the S^{3}E element is applied) or $2S_yI_z$ (when the S^{3}E element is not applied, note that $I = {}^1$H and $S = {}^{15}$N in this context). The detected signal is S_xI^{β} (TROSY) or S_xI^{α} (anti-TROSY), with the effective transverse relaxation rates ($R_{2,eff}$) during the relaxation delay (T_{relax}) computed as in the actual measurements. In simulations for CPMG experiments with the [0013]-phase cycle an additional longitudinal relaxation compensation period is included following an approach described previously [47], whereby the magnetization is rotated to the z-axis after the T_{relax} period. In contrast, in constant phase CPMG experiments such relaxation compensation is, in general, not applied, as the correction is smaller and is offset dependent [32]. The numerical simulation programs are available from the authors upon request, and can also be found in a BMRbig entry (https://bmrbig.org/released/bmrbig97).

3. Results and discussion

3.1. Artifacts from CPMG pulse trains of constant phase

Initial TROSY- [37] and TROSY-/anti-TROSY-based ^{15}N CPMG [18] experiments were developed with constant phase CPMG pulse trains, as indicated in Fig. 1A. At the start of the CPMG element magnetization is aligned along the *y*-axis so that CPMG pulses for the first $T_{relax}/2$ of the train are applied with constant phase *y*. The P element in the center of the train interconverts *x*- and *y*-magnetization so that the CPMG pulses in the second portion of train are applied with phase *x*. Simulations have been performed with this CPMG train as a function of offset of the ^{15}N spin from the RF carrier for both TROSY and anti-TROSY schemes (Fig. 1B, 1E), assuming no chemical exchange. In general, $R_{2,eff}$ values are not constant as a function of ν_{CPMG}, in contrast to what would be expected in the absence of chemical exchange, but show deviations that increase with increasing offsets, and only for small offset values are flat profiles obtained. This effect is particularly pronounced for simulations of anti-TROSY-based ^{15}N CPMG experiments, since the intrinsic transverse relaxation rates for the anti-TROSY components of magnetization are substantially larger than for the corresponding TROSY components, especially in the case of biomolecules with high molecular weights and applications at high magnetic fields. For 'typical' NMR probes, ^{15}N pulses can safely be applied with maximal field strengths of 5–6 kHz so that even modest ^{15}N offsets on the order of 1 kHz (10 ppm at 1 GHz) can lead to significant artifacts. Enhancements in robustness to RF field inhomogeneity and pulse imperfections are also desired, as illustrated in Fig. 1C, 1F

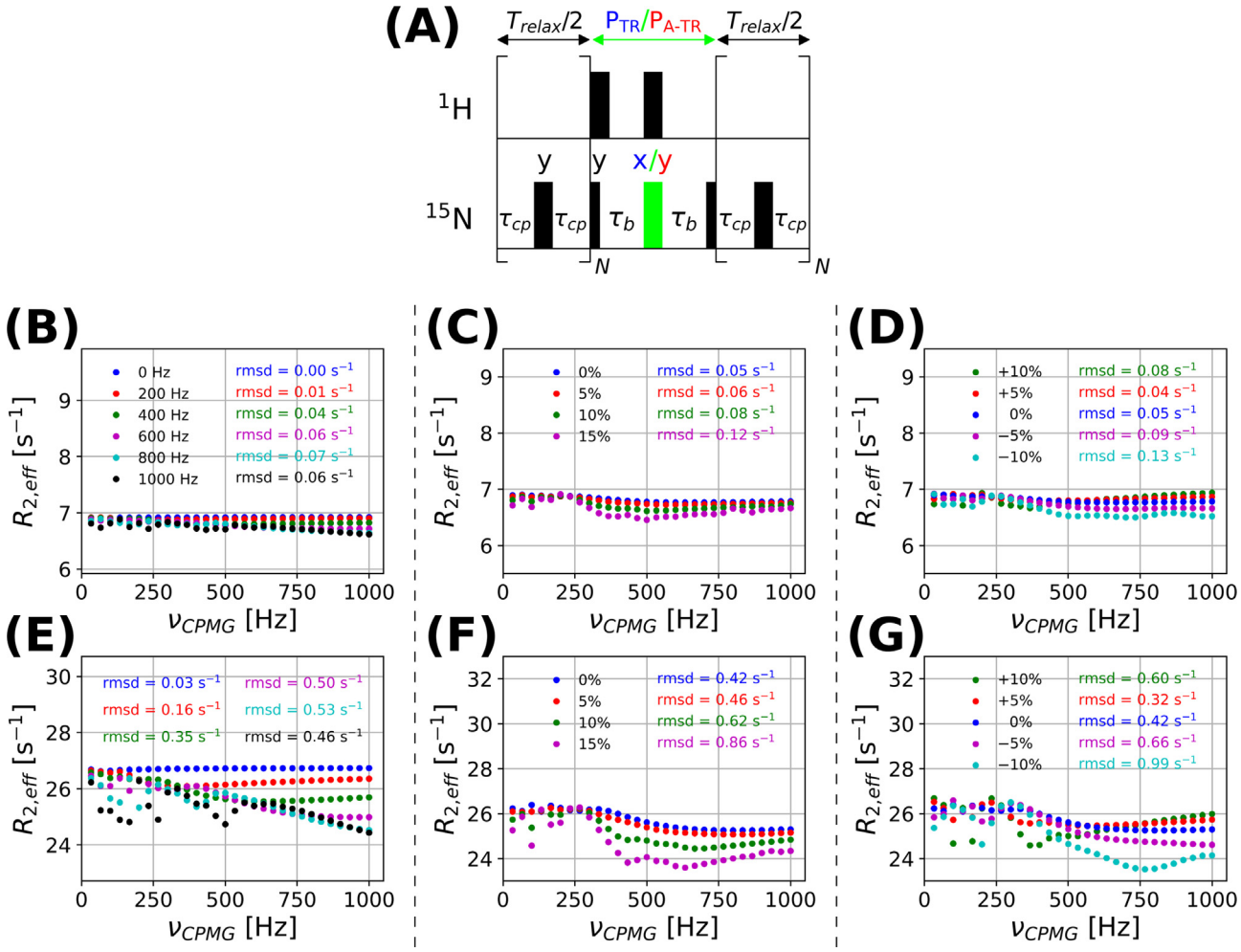

Fig. 1. (A) CPMG pulse train for recording either TROSY- or anti-TROSY-based CPMG relaxation dispersion experiments with constant phase CPMG pulse trains [18]. (B–G) Results from numerical simulations of TROSY- (B–D) and anti-TROSY- (E–G) CPMG experiments with constant phase CPMG pulses. Simulations were performed with the following parameters: $R_1 = 2\ s^{-1}$, $R_2 = 15\ s^{-1}$, $R_{1H} = 4\ s^{-1}$, $\eta_{xy} = 10\ s^{-1}$, $J_{NH} = -93$ Hz, $T_{relax} = 30$ ms, $\nu_1 = 5000$ Hz for CPMG pulses, and in the absence of chemical exchange. Only the TROSY (B–D) or anti-TROSY (E–F) component of magnetization is present at the beginning of the T_{relax} period. (B, E) Evaluation of the effects of ^{15}N offsets; offsets ranging from 0 to 1000 Hz are systematically explored and distinguished by color in each panel, with the root-mean-square deviation (RMSD) value of each profile (relative to the best fit horizontal line) indicated with the same color. (C, F) Evaluation of the performance of pulse trains in the presence of RF inhomogeneity. A constant ^{15}N offset of 500 Hz was used. To account for RF field inhomogeneity, 10 independent calculations were performed with different B_1 fields evenly spaced between $\pm\ 2\sigma$ around the mean, where σ represents the standard deviation of the B_1 field distribution. The results from these 10 calculations are then averaged using the appropriate coefficients assuming a Gaussian profile. Various sizes of RF field inhomogeneity are assumed in the simulation, given by the ratio of σ/ν_1, and indicated with distinct colors in each panel. The RMSD value of each curve is also reported with the same color scheme in each panel. (D, G) Simulations where the CPMG pulse duration, pw_{180}, is set to 10 % or 5 % longer or shorter than the correct value, or at the correct value ($=1/(2\nu_1)$), as indicated by color in each panel. A constant ^{15}N offset of 500 Hz was used. The RMSD value of each profile is indicated using the same color scheme.

and 1D, 1G, respectively, where CPMG profiles are not flat. The importance of designing an improved CPMG element with respect to pulse imperfections is thus clear.

3.2. The design of a TROSY/anti-TROSY CPMG train with a [0013]-phase cycle

One elegant strategy for minimizing artifacts arising from off-resonance effects involves the implementation of a suitably phase cycled CPMG pulse train, using [0013]- [32] or XY- [48] schemes. In general, when the magnetization is either along the *x*- or the *y*-axis at the start of the CPMG relaxation period the [0013]-phase cycle is preferred. Such a scheme has been successfully incorporated into ^{15}N single-quantum experiments such as ST-CW-CPMG and PD-CPMG [33,49], showing improved performance in the presence of off-resonance effects, RF field inhomogeneity, and pulse imperfections compared with other commonly used ^{15}N CPMG experiments. In TROSY- and anti-TROSY-based ^{15}N CPMG experiments, where *x*- or *y*-^{15}N magnetization is initially present, use of the [0013]-phase cycle is expected to enhance the performance of these experiments as well.

Incorporating the [0013]-phase cycle into the ^{15}N ST-CW-CPMG experiment was relatively straightforward [33], as the complete CPMG block in this case comprises a simple train of pulses. Slightly more complex pulse schemes have been developed whereby CPMG pulse trains are divided into two half periods, separated by a single 180° pulse, such as for the ^{15}N CW-CPMG experiment [35] and the ^{1}H single- and triple-quantum sequences using ^{13}CH$_3$-labeled methyl groups as probes [24,25]. The situation is more involved in the present application, as shown in Fig. 2, where an S^{3}CT selective inversion element (P element) [50] is applied in the middle of the CPMG pulse train which (partially) suppresses cross-relaxation between TROSY and anti-TROSY magnetization [37,51]. In what follows we describe how the relative phase values, ψ_1 and ψ_2, of the CPMG pulses are chosen.

The evolution of an *I*–*S* two-spin spin system ($I = {}^1$H and $S = {}^{15}$N) during the CPMG pulse train of Fig. 2 can be described using the product operator formalism [52] and following the theoretical framework delineated in a previous publication [18]. The evolution of magnetization is given by the superoperator $\hat{\hat{R}}$ in Liouville space

$$\hat{\hat{R}} = \hat{\hat{K}}'\hat{\hat{P}}\hat{\hat{K}} \tag{1}$$

where superoperators $\hat{\hat{K}}$ and $\hat{\hat{K}}'$ describe the evolution during the first and second halves of the CPMG pulse train, respectively, with

$$\hat{\hat{K}} = \prod_{j=1}^{N} \exp(-i(2\pi J_{IS}\hat{\hat{I}}_Z\hat{\hat{S}}_Z + \Delta\hat{\hat{S}}_Z)\tau_{cp}) \exp(-i(\omega_1\hat{\hat{S}}_{\psi_1^j} + \Delta\hat{\hat{S}}_Z)pw_{180}) \times \exp(-i(2\pi J_{IS}\hat{\hat{I}}_Z\hat{\hat{S}}_Z + \Delta\hat{\hat{S}}_Z)\tau_{cp}) \tag{2}$$

$$\hat{\hat{K}}' = \prod_{j=1}^{N} \exp(-i(2\pi J_{IS}\hat{\hat{I}}_Z\hat{\hat{S}}_Z + \Delta\hat{\hat{S}}_Z)\tau_{cp}) \exp(-i(\omega_1\hat{\hat{S}}_{\psi_2^j} + \Delta\hat{\hat{S}}_Z)pw_{180}) \times \exp(-i(2\pi J_{IS}\hat{\hat{I}}_Z\hat{\hat{S}}_Z + \Delta\hat{\hat{S}}_Z)\tau_{cp}) \tag{3}$$

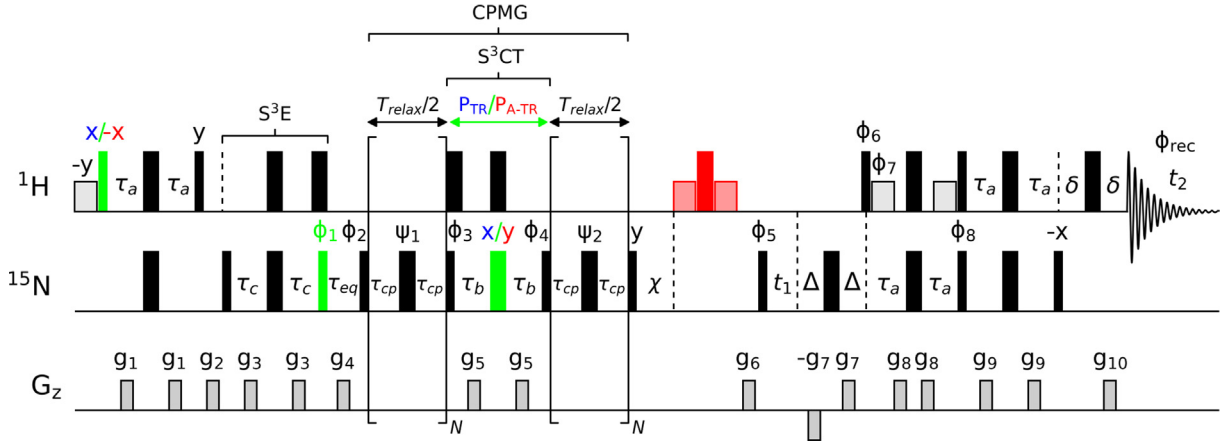

Fig. 2. Pulse schemes of the ^{15}N [0013] TROSY-CPMG and [0013] anti-TROSY-CPMG relaxation dispersion experiments. 90° (180°) rectangular pulses on ^{1}H and ^{15}N channels are denoted by *narrow* (*wide*) *bars* and applied at maximum available power, with the exception of ^{15}N pulses during the CPMG relaxation dispersion period, which are typically 1–2 dB lower than the maximal available power and in the range of 5–6 kHz. Selective ^{1}H pulses applied on water typically have a duration of ~1.5 ms. All pulses are applied with phase *x* unless otherwise indicated. The ^{1}H carrier is placed on resonance with the water line (~4.7 ppm) and the ^{15}N carrier is placed in the center of the amide region (~119 ppm). The delays used are: τ_a = 2.38 ms, τ_b = 2.68 ms ($=1/|4J_{NH}|$), τ_c = 1.34 ms ($=1/|8J_{NH}|$), Δ = 850 μs, δ = 500 μs, τ_{eq} = 2–5 ms, $\tau_{cp} = (T_{relax}/(2N) - 0.75\times pw_{180})/2$ where pw_{180} is the length of each refocusing CPMG pulse and the delay time $\chi = 0.5\times(N_{max} - N)\times pw_{180}$ compensates for longitudinal relaxation of ^{15}N magnetization during the CPMG pulses (N_{max} is the largest value of *N*). The delay τ_{eq} allows for equilibration of magnetization [35]. The *red* colored pulses (converting anti-TROSY to TROSY magnetization) are applied only for the anti-TROSY-based experiments, *blue* or *red* colored phases are applied for TROSY- or anti-TROSY-based experiments respectively, *green* colored pulses are applied with different phases in TROSY- or anti-TROSY-based experiments. The phase cycle is ϕ_1 = 45° (TROSY-based) or 315° (anti-TROSY-based); $\phi_2 = x, -x$; $\phi_3 = y, -y, -y, y$; $\phi_4 = x, -x, -x, x$; $\phi_5 = 2(y), 2(-x), 2(-y), 2(x)$; $\phi_6 = y$; $\phi_7 = -y$; $\phi_8 = -y$; $\phi_{rec} = -y, y, -x, x, y, -y, x, -x$. Quadrature detection in the F_1 dimension is achieved by inverting the phases of ϕ_6, ϕ_7, ϕ_8 together with the sign of gradient g_7 [58], and changing ϕ_5 to $2(y)$, $2(x)$, $2(-y)$, $2(-x)$. Note that the phases are specific to Bruker spectrometers; for Varian spectrometers, phase shifts (relative to phase *x*) should be inverted (i.e., *y* and $-y$ interchanged). A minimum four step cycle is recommended for optimal TROSY selection, although a two step cycle is sufficient when coherence selection gradients (g_7, g_{10}) are applied, as illustrated. When coherence selection gradients are not applied (without "-Dgd_sel" in ZGOPTNS), a minimum four step phase cycle is required. The phases ψ_1/ψ_2 are used for implementing the [0013]-phase scheme [32] for cycling the CPMG pulses. Phase ψ_1 is incremented with the cycle ($y, y, x, -x$) for each successive pulse, such that for $N = 3$ the phases of the first, second and third pulses in the first half of the CPMG pulse train are *y*, *y* and *x*, respectively, and ψ_2 is decremented starting from the final ψ_1 phase with *x* and *y* interchanged (or $-x$ and $-y$ interchanged), such that for $N = 3$ the phases of the first, second and third pulses in the second half of the CPMG pulse train are *y*, *x* and *x*, respectively [24,25]. Gradients are applied with the following durations (ms) and strengths (in % maximum): g_1: (0.256, 25 %), g_2: (1.0, −70 %), g_3: (0.256, 25 %), g_4: (1.0, −70 %), g_5: (0.3, 30 %), g_6: (1.0, 90 %), g_7: (0.625, 80 %), g_8: (0.256, 60 %), g_9: (0.256, 15 %), g_{10}: (0.256, 39.6 %). Note that the strength of g_{10} may need to be optimized for maximum sensitivity for each probe. Heating compensation is implemented to ensure that the amount of sample heating arising from the CPMG pulses and potential ^{15}N channel detuning is independent of ν_{CPMG} (via "-DN_comp" in ZGOPTNS), although for applications involving Bruker cryo-probes we have found this to be minimal. The 180° ^{15}N pulse in the middle of S^{3}CT element can be replaced with a REBURP shaped pulse [59] for larger bandwidth coverage (via "-Dreb_flg" in ZGOPTNS). The pulse sequence code for Bruker spectrometers is included in Supplementary material, and can also be found in a BMRbig entry (https://bmrbig.org/released/bmrbig97).

In Eqs. (2) and (3) ψ_1^j and ψ_2^j are the phases of the j-th pulse in the first and second halves of pulse train, respectively. The operators for the S^{3}CT selective inversion elements are given by

$$\hat{P}_{TR} = \exp(-i\frac{\pi}{2}\hat{S}_X)\exp(-i(2\pi J_{IS}\hat{I}_Z\hat{S}_Z + \Delta\hat{S}_Z)\tau_b)\exp(-i\pi\hat{S}_X)\exp(-i\pi\hat{I}_X) \times \exp(-i(2\pi J_{IS}\hat{I}_Z\hat{S}_Z + \Delta\hat{S}_Z)\tau_b)\exp(-i\pi\hat{I}_X)\exp(-i\frac{\pi}{2}\hat{S}_Y) \quad (4)$$

$$\hat{P}_{A\text{-}TR} = \exp(-i\frac{\pi}{2}\hat{S}_X)\exp(-i(2\pi J_{IS}\hat{I}_Z\hat{S}_Z + \Delta\hat{S}_Z)\tau_b)\exp(-i\pi\hat{S}_Y)\exp(-i\pi\hat{I}_X) \times \exp(-i(2\pi J_{IS}\hat{I}_Z\hat{S}_Z + \Delta\hat{S}_Z)\tau_b)\exp(-i\pi\hat{I}_X)\exp(-i\frac{\pi}{2}\hat{S}_Y) \quad (5)$$

for the TROSY (Eq. (4)) and anti-TROSY (Eq. (5)) experiments, where $\Delta\hat{S}_Z$ is the Zeeman superoperator for spin S, Δ (rad/sec) is the offset of spin S from the RF carrier in the rotating frame, $2\pi J_{IS}\hat{I}_Z\hat{S}_Z$ is the scalar coupling superoperator connecting spins I and S, ω_1 is RF field strength (rad/sec) for spin S, and pw_{180} is the duration of each refocusing CPMG pulse. When $\tau_b = 1/(4J_{IS})$, $\hat{P}_{TR}$ and $\hat{P}_{A\text{-}TR}$ can be simplified as

$$\hat{P}_{TR} = \exp(-i\frac{\pi}{2}\hat{S}_X)\exp(-i\pi\hat{I}_Z\hat{S}_Z)\exp(-i\pi\hat{S}_X)\exp(-i\frac{\pi}{2}\hat{S}_Y) \quad (6)$$

$$\hat{P}_{A\text{-}TR} = \exp(-i\frac{\pi}{2}\hat{S}_X)\exp(-i\pi\hat{I}_Z\hat{S}_Z)\exp(-i\pi\hat{S}_Y)\exp(-i\frac{\pi}{2}\hat{S}_Y) \quad (7)$$

and the evolution of TROSY, $\hat{S}^{\beta}(t) = \begin{pmatrix} S_X I^{\beta}(t) \\ S_Y I^{\beta}(t) \\ S_Z I^{\beta}(t) \end{pmatrix}$, or anti-TROSY, $\hat{S}^{\alpha}(t) = \begin{pmatrix} S_X I^{\alpha}(t) \\ S_Y I^{\alpha}(t) \\ S_Z I^{\alpha}(t) \end{pmatrix}$, coherences from the P element in the TROSY- or anti-TROSY-based experiments, is given by

$$\hat{P}_{TR}\hat{S}^{\beta}(t) = \hat{P}_{TR}\begin{pmatrix} S_X I^{\beta}(t) \\ S_Y I^{\beta}(t) \\ S_Z I^{\beta}(t) \end{pmatrix} = \begin{pmatrix} -S_Y I^{\beta}(t) \\ -S_X I^{\beta}(t) \\ -S_Z I^{\beta}(t) \end{pmatrix},$$
$$\hat{P}_{A\text{-}TR}\hat{S}^{\alpha}(t) = \hat{P}_{A\text{-}TR}\begin{pmatrix} S_X I^{\alpha}(t) \\ S_Y I^{\alpha}(t) \\ S_Z I^{\alpha}(t) \end{pmatrix} = \begin{pmatrix} -S_Y I^{\alpha}(t) \\ -S_X I^{\alpha}(t) \\ -S_Z I^{\alpha}(t) \end{pmatrix} \quad (8)$$

Thus, the P element is equivalent to a –90° rotation along the z-axis (*i.e.*, 90° clockwise) followed by an additional 180° rotation along the y-axis, so that we can define the corresponding operator as $\hat{P} = \exp(-i\pi\hat{S}_Y)\exp(i\frac{\pi}{2}\hat{S}_Z)$. Note that the pair of 90° ^{15}N flanking pulses in the S^{3}CT selective inversion element helps to eliminate unwanted magnetization components that arise when this pulse scheme is used to measure RDC values (D_{IS}) in the excited state [18], where the magnitude of the ^{1}H–^{15}N effective coupling, J_{eff} (= J_{IS} + D_{IS}), varies from one residue to the next, that is $J_{eff} \neq J_{IS}$. Focusing on Eq. (1) above we can write,

$$\hat{R} = \hat{K}'\hat{P}\hat{K} = \hat{K}'(\hat{P}\hat{K}\hat{P}^{-1})\hat{P} = \hat{K}'\hat{K}''\hat{P} \quad (9)$$

where $\hat{K}'' = \hat{P}\hat{K}\hat{P}^{-1}$ is given by

$$\begin{aligned}
&\exp(-i\pi\hat{S}_Y)\exp(i\tfrac{\pi}{2}\hat{S}_Z)\hat{K}\exp(-i\tfrac{\pi}{2}\hat{S}_Z)\exp(i\pi\hat{S}_Y)\\
&= \exp(-i\pi\hat{S}_Y)\exp(i\frac{\pi}{2}\hat{S}_Z)\left\{\prod_{j=1}^{N}\left[\exp(-i(2\pi J_{IS}\hat{I}_Z\hat{S}_Z + \Delta\hat{S}_Z)\tau_{cp})\exp(-i(\omega_1\hat{S}_{\psi_1^j} + \Delta\hat{S}_Z)pw_{180})\exp(-i(2\pi J_{IS}\hat{I}_Z\hat{S}_Z + \Delta\hat{S}_Z)\tau_{cp})\right]\right\}\exp(-i\frac{\pi}{2}\hat{S}_Z)\exp(i\pi\hat{S}_Y)\\
&= \prod_{j=1}^{N}\left\{\exp(-i\pi\hat{S}_Y)\exp(i\frac{\pi}{2}\hat{S}_Z)\left[\exp(-i(2\pi J_{IS}\hat{I}_Z\hat{S}_Z + \Delta\hat{S}_Z)\tau_{cp})\exp(-i(\omega_1\hat{S}_{\psi_1^j} + \Delta\hat{S}_Z)pw_{180})\exp(-i(2\pi J_{IS}\hat{I}_Z\hat{S}_Z + \Delta\hat{S}_Z)\tau_{cp})\right]\exp(-i\frac{\pi}{2}\hat{S}_Z)\exp(i\pi\hat{S}_Y)\right\}\\
&= \prod_{j=1}^{N}\left\{\exp(i(2\pi J_{IS}\hat{I}_Z\hat{S}_Z + \Delta\hat{S}_Z)\tau_{cp})\left[\exp(-i\pi\hat{S}_Y)\exp(i\frac{\pi}{2}\hat{S}_Z)\exp(-i(\omega_1\hat{S}_{\psi_1^j} + \Delta\hat{S}_Z)pw_{180})\exp(-i\frac{\pi}{2}\hat{S}_Z)\exp(i\pi\hat{S}_Y)\right]\exp(i(2\pi J_{IS}\hat{I}_Z\hat{S}_Z + \Delta\hat{S}_Z)\tau_{cp})\right\}\\
&= \prod_{j=1}^{N}\left[\exp(i(2\pi J_{IS}\hat{I}_Z\hat{S}_Z + \Delta\hat{S}_Z)\tau_{cp})\exp(i(\omega_1\hat{S}_{\psi_2^{Q(j)}} + \Delta\hat{S}_Z)pw_{180})\exp(i(2\pi J_{IS}\hat{I}_Z\hat{S}_Z + \Delta\hat{S}_Z)\tau_{cp})\right]\\
&= \prod_{j=1}^{N}\left[\exp(-i(2\pi J_{IS}\hat{I}_Z\hat{S}_Z + \Delta\hat{S}_Z)\tau_{cp})\exp(-i(\omega_1\hat{S}_{\psi_2^{Q(j)}} + \Delta\hat{S}_Z)pw_{180})\exp(-i(2\pi J_{IS}\hat{I}_Z\hat{S}_Z + \Delta\hat{S}_Z)\tau_{cp})\right]^{-1}\\
&= \left[\prod_{j=1}^{N}\exp(-i(2\pi J_{IS}\hat{I}_Z\hat{S}_Z + \Delta\hat{S}_Z)\tau_{cp})\exp(-i(\omega_1\hat{S}_{\psi_2^{Q(N-j+1)}} + \Delta\hat{S}_Z)pw_{180})\exp(-i(2\pi J_{IS}\hat{I}_Z\hat{S}_Z + \Delta\hat{S}_Z)\tau_{cp})\right]^{-1}
\end{aligned} \quad (10)$$

Note that we have used the relation $\hat{P}\hat{S}_{\psi_1^j}\hat{P}^{-1} = -\hat{S}_{\psi_2^{Q(j)}}$, or alternatively that,

$$\exp(-i\pi\hat{S}_Y)\exp(i\frac{\pi}{2}\hat{S}_Z)\exp(-i\theta\hat{S}_{\psi_1^j})\exp(-i\frac{\pi}{2}\hat{S}_Z)\exp(i\pi\hat{S}_Y) = \exp(i\theta\hat{S}_{\psi_2^{Q(j)}}) = \left[\exp(-i\theta\hat{S}_{\psi_2^{Q(j)}})\right]^{-1} \quad (11)$$

in Eq. (10) above (Line 5), where θ is an arbitrary rotation angle. We search for $Q(j)$ such that $\hat{K}'' = (\hat{K}')^{-1}$ since then,

$$\hat{R} = \hat{K}'\hat{P}\hat{K} = \hat{K}'\hat{K}''\hat{P} = \hat{K}'(\hat{K}')^{-1}\hat{P} = \exp(-i\pi\hat{S}_Y)\exp(i\frac{\pi}{2}\hat{S}_Z) \quad (12)$$

and the net evolution due to the CPMG train becomes immune to pulse imperfections. That is, any imperfections in the first half of the train are completely undone by the action of the second half of the CPMG element. Comparing $\hat{K}''$ (Eq. (10), last line) with $(\hat{K}')^{-1}$ (see Eq. (3)) establishes that a necessary condition is that $Q(N\text{–}j + 1) = j$, or, alternatively, $Q(j) = N\text{–}j + 1$. Thus, ψ_1 and ψ_2 values must be chosen according to the following relationship: $\begin{pmatrix} \psi_1^j \\ \psi_2^{N-j+1} \end{pmatrix} \in \left\{\begin{pmatrix} x \\ y \end{pmatrix}, \begin{pmatrix} y \\ x \end{pmatrix}, \begin{pmatrix} -x \\ -y \end{pmatrix}, \begin{pmatrix} -y \\ -x \end{pmatrix}\right\}$, which follows directly from Eq. (11). The above discussion establishes that evolution from chemical shifts and scalar couplings can be effectively refocused by employing a judicious phase cycle in TROSY- and anti-TROSY-based CPMG experiments. This refocusing effect does, however, require that the P element itself is 'perfect' in that the element executes a perfect series of rotations as indicated in Eqs. (6) and (7) (with τ_b set appropriately to $1/(4J_{IS})$, as described above).

3.3. Further improvements

Fig. 2 illustrates the pulse scheme that has been developed to record robust TROSY/anti-TROSY CPMG relaxation dispersion profiles. In addition to the CPMG train, a number of further modifications have been made over the original sequence [18]. First, we have added the option of applying an S^3E element for spin-state-selective excitation [53] at the start of the pulse scheme. In this manner the initial magnetization prior to the CPMG T_{relax} period is either of the TROSY or anti-TROSY variety, rather than an equal combination of both, which would otherwise ensue in the absence of the selection. We show below that the presence of both TROSY and anti-TROSY components at the start of the CPMG train can cause artifacts when the amide ^{1}H spin-flip rates are large.

To understand the origin of these potential artifacts we consider the evolution of TROSY and anti-TROSY components during a free precession period,

$$\frac{d}{dt}\begin{pmatrix} S_+I^\alpha(t) \\ S_+I^\beta(t) \end{pmatrix} = \begin{pmatrix} -i\pi J_{IS} - R_{2,A\text{-}TR} & R_{1H}/2 \\ R_{1H}/2 & i\pi J_{IS} - R_{2,TR} \end{pmatrix}\begin{pmatrix} S_+I^\alpha(t) \\ S_+I^\beta(t) \end{pmatrix} \tag{13}$$

where $S_+ = S_X + iS_Y$, $R_{2,TR}$ ($= R_2 - \eta_{xy} + R_{1H}/2$) and $R_{2,A\text{-}TR}$ ($= R_2 + \eta_{xy} + R_{1H}/2$) are the transverse relaxation rates of TROSY and anti-TROSY components, respectively, η_{xy} is the ^{1}H–^{15}N dipole–dipole/^{15}N chemical shift anisotropy (DD/CSA) cross-correlated relaxation rate, and R_{1H} is the amide ^{1}H spin-flip rate that interconverts TROSY and anti-TROSY magnetization components. In the slow CPMG pulsing limit ($\nu_{CPMG} \ll J_{IS}$), the off-diagonal elements can be discarded via the secular approximation,

$$\frac{d}{dt}\begin{pmatrix} S_+I^\alpha(t) \\ S_+I^\beta(t) \end{pmatrix} = \begin{pmatrix} -i\pi J_{IS} - R_{2,A\text{-}TR} & 0 \\ 0 & i\pi J_{IS} - R_{2,TR} \end{pmatrix}\begin{pmatrix} S_+I^\alpha(t) \\ S_+I^\beta(t) \end{pmatrix} \tag{14}$$

since the precession frequency difference between the TROSY and anti-TROSY components is generally much larger than R_{1H}. Consequently, TROSY and anti-TROSY components relax independently, with apparent relaxation rates of $R_{2,TR}$ and $R_{2,A\text{-}TR}$ during the T_{relax} period. In the fast CPMG pulsing limit ($\nu_{CPMG} \gg J_{IS}$), the precession frequency difference between TROSY and anti-TROSY components is eliminated, so that the spin system evolves as

$$\frac{d}{dt}\begin{pmatrix} S_+I^\alpha(t) \\ S_+I^\beta(t) \end{pmatrix} = \begin{pmatrix} -R_{2,A\text{-}TR} & R_{1H}/2 \\ R_{1H}/2 & -R_{2,TR} \end{pmatrix}\begin{pmatrix} S_+I^\alpha(t) \\ S_+I^\beta(t) \end{pmatrix} = \hat{\Gamma}\begin{pmatrix} S_+I^\alpha(t) \\ S_+I^\beta(t) \end{pmatrix} \tag{15}$$

In the TROSY-based CPMG experiment the S^3CT element leads to the conversion of magnetization components via $\hat{P}_{TR}\begin{pmatrix} S_YI^\alpha(t) \\ S_YI^\beta(t) \end{pmatrix} = \begin{pmatrix} S_XI^\alpha(t) \\ -S_XI^\beta(t) \end{pmatrix}$, so that the evolution of the spin system during T_{relax} can be described as

$$\begin{pmatrix} S_XI^\alpha(T_{relax}) \\ S_XI^\beta(T_{relax}) \end{pmatrix} = \exp(\hat{\Gamma}T_{relax}/2)\begin{pmatrix} 1 & 0 \\ 0 & -1 \end{pmatrix}\exp(\hat{\Gamma}T_{relax}/2)\begin{pmatrix} S_YI^\alpha(0) \\ S_YI^\beta(0) \end{pmatrix} \tag{16}$$

where we have assumed that both TROSY and anti-TROSY magnetization components are present at the start of the CPMG period. The evolution of magnetization as per Eq. (16), via $\hat{U} = \exp(\hat{\Gamma}T_{relax}/2)\begin{pmatrix} 1 & 0 \\ 0 & -1 \end{pmatrix}\exp(\hat{\Gamma}T_{relax}/2)$, can be simplified by defining

$$\hat{\Gamma}' = \begin{pmatrix} 1 & 0 \\ 0 & -1 \end{pmatrix}\begin{pmatrix} -R_{2,A\text{-}TR} & R_{1H}/2 \\ R_{1H}/2 & -R_{2,TR} \end{pmatrix}\begin{pmatrix} 1 & 0 \\ 0 & -1 \end{pmatrix} = \begin{pmatrix} -R_{2,A\text{-}TR} & -R_{1H}/2 \\ -R_{1H}/2 & -R_{2,TR} \end{pmatrix} \tag{17}$$

so that the superoperator $\hat{U} = \exp(\hat{\Gamma}T_{relax}/2)\begin{pmatrix} 1 & 0 \\ 0 & -1 \end{pmatrix}\exp(\hat{\Gamma}T_{relax}/2)$ becomes

$$\hat{U} = \exp(\hat{\Gamma}T_{relax}/2)\exp(\hat{\Gamma}'T_{relax}/2)\begin{pmatrix} 1 & 0 \\ 0 & -1 \end{pmatrix} \tag{18}$$

Using the Baker–Campbell–Hausdorff (BCH) relationship with retention of terms to second order in time yields

$$\begin{aligned} \hat{U} &\simeq \exp\left(\frac{\hat{\Gamma}T_{relax}}{2} + \frac{\hat{\Gamma}'T_{relax}}{2} + \frac{1}{2}\left[\frac{\hat{\Gamma}T_{relax}}{2}, \frac{\hat{\Gamma}'T_{relax}}{2}\right]\right)\begin{pmatrix} 1 & 0 \\ 0 & -1 \end{pmatrix} \\ &= \exp\begin{pmatrix} -R_{2,A\text{-}TR}T_{relax} & \eta_{xy}R_{1H}T_{relax}^2/4 \\ -\eta_{xy}R_{1H}T_{relax}^2/4 & -R_{2,TR}T_{relax} \end{pmatrix}\begin{pmatrix} 1 & 0 \\ 0 & -1 \end{pmatrix} \\ &\simeq \begin{pmatrix} e^{-R_{2,A\text{-}TR}T_{relax}} & \frac{(e^{-R_{2,TR}T_{relax}} - e^{-R_{2,A\text{-}TR}T_{relax}})R_{1H}T_{relax}}{8} \\ \frac{(e^{-R_{2,A\text{-}TR}T_{relax}} - e^{-R_{2,TR}T_{relax}})R_{1H}T_{relax}}{8} & e^{-R_{2,TR}T_{relax}} \end{pmatrix} \\ &\times \begin{pmatrix} 1 & 0 \\ 0 & -1 \end{pmatrix} \end{aligned} \tag{19}$$

Thus, for the initial condition $\begin{pmatrix} S_YI^\alpha(0) \\ S_YI^\beta(0) \end{pmatrix} = \begin{pmatrix} 1 \\ -1 \end{pmatrix}$, which is operative in the case that an S^3E element is not applied prior to T_{relax} (*i.e.*, initial ^{15}N magnetization is antiphase) the apparent decay of TROSY and anti-TROSY components is given by $\exp(-R_{2,TR}T_{relax})\left[1 + \frac{(e^{-2\eta_{xy}T_{relax}} - 1)R_{1H}T_{relax}}{8}\right]$ and $\exp(-R_{2,A\text{-}TR}T_{relax})\left[1 + \frac{(e^{2\eta_{xy}T_{relax}} - 1)R_{1H}T_{relax}}{8}\right]$, respectively, deviating from $\exp(-R_{2,TR}T_{relax})$ and $\exp(-R_{2,A\text{-}TR}T_{relax})$. Thus, in the case of TROSY-based experiments and for initial ν_{CPMG} rates ($\nu_{CPMG} \ll J_{IS}$) $R_{2,eff} \simeq R_{2,TR}$, while for larger ν_{CPMG} values the effective relaxation increases, giving rise to a profile that is not flat, even in the absence of chemical exchange. By contrast, introduction of the S^3E element ensures that only TROSY or anti-TROSY components are present at the beginning of T_{relax}, effectively suppressing artificial relaxation dispersion arising from cross-relaxation between the TROSY and anti-TROSY components. Although the intrinsic sensitivity of the CPMG experiment is slightly reduced by the additional $1/|4J_{NH}|$ ($\simeq 2.68$ ms) duration of the S^3E element, its use is likely to be worthwhile, especially in studies of systems with relatively large amide ^{1}H spin-flip rates, such as might be the case with applications involving fully protonated proteins, samples with rapid solvent exchange, or biomolecules with high molecular weights. The combination of ^{1}H spin flips, coupled with large differences between the relaxation rates of TROSY and anti-TROSY components, such as would be the case for applications involving large biomolecules at high magnetic fields, can lead to artifactual dispersion profiles (see discussion above and further discussion below). Notably, by applying S^3E and S^3CT elements together, each of the TROSY and anti-TROSY components can be regarded as essentially independent, both behaving as in-phase single quantum coherences during T_{relax}, allowing for the robust extraction of chemical shift differences as for regular non-TROSY CPMG relaxation dispersion experiments. Indeed, the more favorable relaxation of TROSY magnetization is likely to translate into increased accuracy of shift differences than for non-TROSY versions of the experiment, especially when exchange rates are slow [37].

A second improvement with the current version of the experiment concerns compensation for evolution during the CPMG pulses. In a 'typical' CPMG scheme, where all phases are constant, the interpulse delay, $2\tau_{cp}$, is calculated as $2\tau_{cp} = T_{relax}/(2N) - pw_{180}$, where pw_{180} is the CPMG pulse width, with no compensation for the relaxation of the component of magnetization along the z-axis during each pulse. Yip and Zuiderweg [32] have shown that, in general, there is no single delay that can compensate for the evolution of magnetization during pulses of constant phase CPMG trains, as the effective relaxation during each pulse is a function of the offset of each spin. In contrast, the situation is much simpler for [0013]-phase cycles [32]. One possibility is to correct for the evolution, post-acquisition, according to the relation [32]

$$R_{2,TR/A\text{-}TR,eff}^{corrected} = R_{2,TR/A\text{-}TR,eff} + \frac{(R_{2,TR/A\text{-}TR} - R_{1,TR/A\text{-}TR}) \times N \times pw_{180}}{2T_{relax}} \tag{20}$$

for the [0013]-TROSY/[0013]-anti-TROSY (*TR/A-TR*) experiments, as was suggested in the context of the ^{15}N ST-CW-CPMG experiment [33]. A simpler approach is to modify the interpulse delay as $2\tau_{cp} = T_{relax}/(2N) - 0.75 \times pw_{180}$. Consider on-resonance magnetization initially along the *x*-axis under the sequential application of four CPMG pulses with phases *x/x/y/–y*. In this case, the magnetization remains in the transverse plane during the first two *x*-pulses, while it resides in the transverse plane for only 50 % of the time during the subsequent two *y/–y*-pulses, so that effectively the magnetization is transverse for 3/4 of each pulse. A comparable scenario holds for off-resonance magnetization, provided that the offset is not excessively large [32]. With this 'new' value for τ_{cp}, post-acquisition processing to 'flatten' out the dispersion profiles is no longer required. Additionally, we have included compensation for the time that magnetization is along the *z*-axis during application of the CPMG pulses, as illustrated in Fig. 2, and described previously [47]. It is noteworthy that the software package *ChemEx* [44], which is based on numerical calculations of the evolution of magnetization during a user-defined CPMG pulse train, can readily account for the modifications described here.

3.4. Numerical simulations highlight benefits of the new scheme

Fig. 3A–F present computations of TROSY (A–C) and anti-TROSY (D–F) dispersion profiles (magnetization is either TROSY or anti-TROSY at the start of the relaxation element), as a function of resonance offset (A, D), RF inhomogeneity (B, E), or pulse miscalibration (C, F) using the [0013]-CPMG train of Fig. 2. In comparison with the corresponding computations for a constant phase CPMG element (Fig. 1) the improvements are considerable. In Fig. 3G, 3H the simple modification to the CPMG interpulse delay ($2\tau_{cp} = T_{relax}/(2N) - 0.75 \times pw_{180}$) along with compensation for the time that magnetization resides along the *z*-axis during the CPMG pulses, discussed above, are shown to result in much flatter dispersion profiles (no exchange), relative to the subtraction of $0.5 \times pw_{180}$ from each τ_{cp} delay and

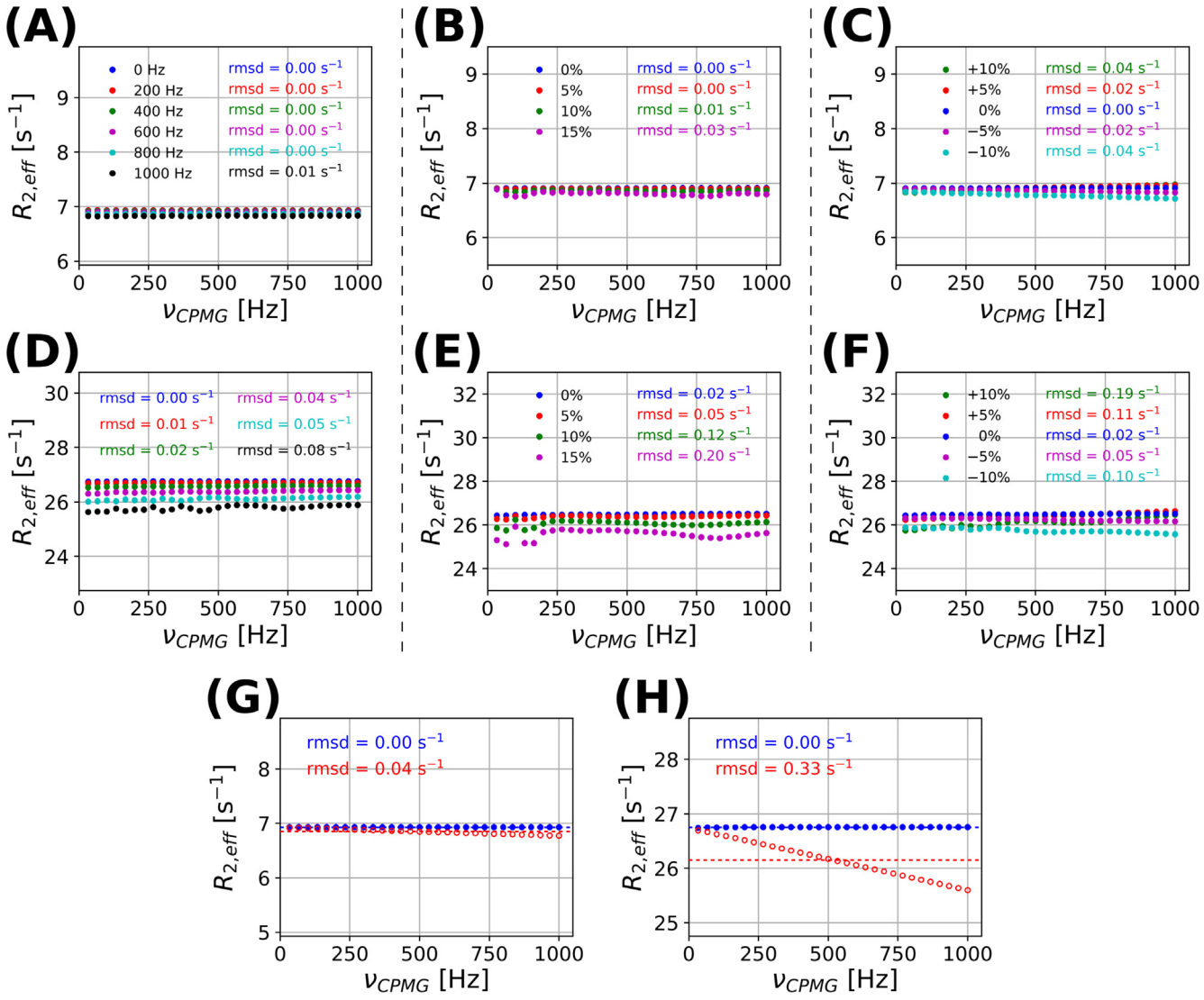

Fig. 3. Simulated dispersion profiles for ^{15}N [0013] TROSY- (panels A–C,G) and [0013] anti-TROSY- (panels D–F,H) CPMG pulse trains using the scheme of Fig. 2. All simulation parameters are as in Fig. 1, with panels (A, D), (B, E), and (C, F) evaluating the effects of offset, RF inhomogeneity, and pulse miscalibration on the resulting profiles, respectively. See Fig. 1 for a comparison with results generated for a constant phase CPMG train. Panels G and H show TROSY (G) and anti-TROSY (H) profiles for on-resonance magnetization where the interpulse delay, $2\tau_{cp}$, is set to $2\tau_{cp} = T_{relax}/(2N) - 0.75 \times pw_{180}$ (*blue dots*) and using a scheme which compensates for the time magnetization resides along the *z*-axis during the CPMG pulses, as illustrated in Fig. 2 and discussed in the text, or $2\tau_{cp} = T_{relax}/(2N) - pw_{180}$ (*red dots*) without compensation for the time spent along the *z*-axis during the pulses, as is typically done in CPMG experiments. The non-zero slope of the $R_{2,eff}$ profile with respect to ν_{CPMG} is clear in these cases. The *dashed lines* in G and H indicate the best fit horizontal lines to the dispersion profiles.

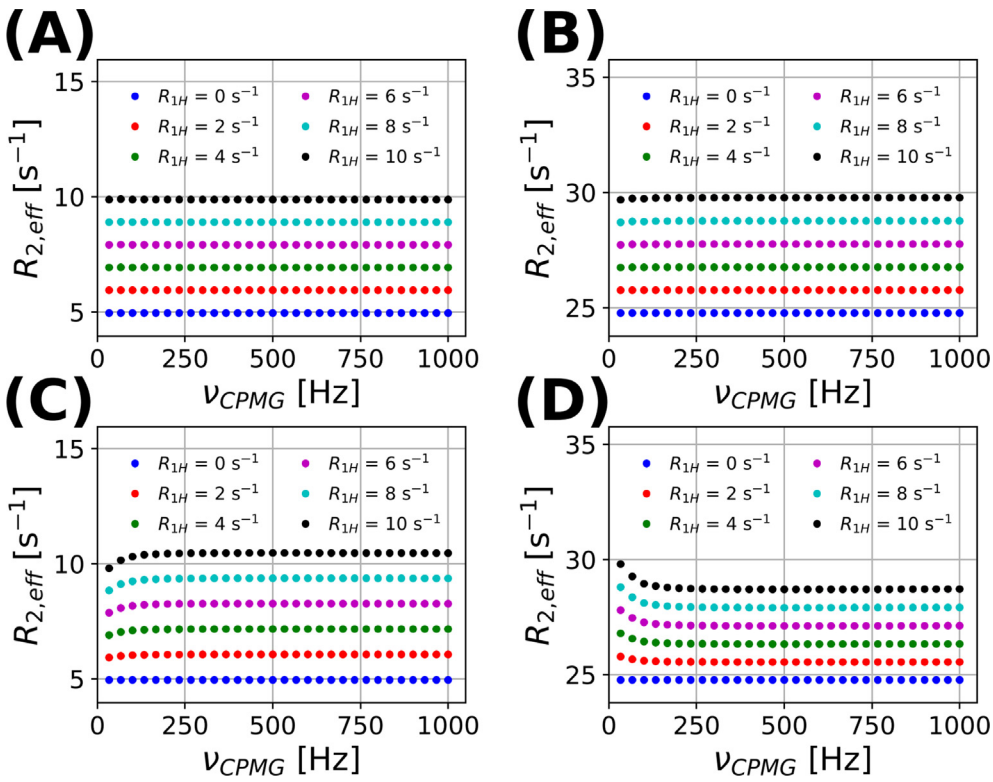

Fig. 4. Simulated CPMG relaxation dispersion profiles for different initial conditions. In panels (A) and (B) computations include an S^3E element immediately prior to the CPMG trains in ^{15}N [0013] TROSY- (A) and anti-TROSY- (B) CPMG profiles. In contrast, panels C and D show results without the S^3E element using TROSY (C) and anti-TROSY (D) sequences ([0013]-phase cycle), respectively. The following parameters were used: R_1 = 2 s^{-1}, R_2 = 15 s^{-1}, η_{xy} = 10 s^{-1}, J_{NH} = –93 Hz, T_{relax} = 30 ms, ν_1 = 5000 Hz for CPMG pulses, and no exchange. Magnetization is on-resonance in all simulations. Profiles with ^1H spin-flip rates (R_{1H}) in the range 0–10 s^{-1} are shown and distinguished by color in each panel.

neglect of differential relaxation of transverse and *z*-magnetization during the pulses. Finally, we have evaluated the utility of the S^3E element by performing simulations as a function of R_{1H} (Eq. (13)). With the initial selection of either the TROSY (Fig. 4A) or anti-TROSY (Fig. 4B) component the dispersion profiles are flat (no exchange) for all values of R_{1H} considered (up to 10 s^{-1}). In contrast, when either of the components is not selected initially, and for $R_{1H} \geq 5$ s^{-1}, noticeable deviations from the expected flat profiles are observed, with the TROSY (anti-TROSY) curves increasing (decreasing) as a function of increasing ν_{CPMG} (Fig. 4C, 4D).

3.5. Experimental validation

The pulse scheme of Fig. 2 has been used to record ^{15}N CPMG relaxation dispersion profiles for a variety of protein samples with different μs–ms timescale dynamics and the results compared with data recorded using other, well-established ^{15}N CPMG experiments, including an earlier version of the TROSY/anti-TROSY sequence with constant phase [18], and the ^{15}N ST-CW-CPMG scheme [33]. Protein L is a model system which is often used in our laboratories to validate new experiments because of the absence of μs–ms timescale exchange processes [54] and, therefore, flat dispersion profiles are expected. Lowering the temperature to 4 °C, as we have done in our studies here, achieves the slow tumbling behavior typical for biomolecules with molecular weights of 15–20 kDa. In the constant phase version of the TROSY- and anti-TROSY-based CPMG experiments [18] prominent artifacts emerge with increasing ^{15}N offset, particularly noticeable in profiles of anti-TROSY coherences due to their elevated intrinsic R_2 rates (Fig. 5). Evaluation based on 56 residues lacking μs–ms timescale dynamics yields a root-mean-square deviation (RMSD) of 0.09 ± 0.03 s^{-1} and 0.12 ± 0.04 s^{-1} for the [0013]-versions of the TROSY- and anti-TROSY-based experiments, respectively, with corresponding RMSD values of 0.11 ± 0.04 s^{-1} and 0.32 ± 0.14 s^{-1} for the constant phase version. These results highlight the superior suppression of artifacts caused by pulse imperfections in the [0013]-TROSY/[0013]-anti-TROSY CPMG experiments of Fig. 2, enabling more accurate identification of dispersions due to chemical exchange process, in particular, when exchange contributions are small.

As a second test, we recorded profiles on a sample of the G48A FynSH3 domain, which shows pronounced signatures of chemical exchange from the interconversion between folded major (ground) and unfolded minor (excited) conformations [40]. Here we have compared results recorded with the ^{15}N [0013] TROSY-CPMG experiment with those obtained from the ^{15}N ST-CW-CPMG sequence. A comprehensive analysis involving 42 residues which exhibit substantial CPMG relaxation dispersions (profiles with $\Delta R_{2,eff}$ (= $R_{2,eff}(\nu_{CPMG}$ = 25 Hz) – $R_{2,eff}(\nu_{CPMG}$ = 1000 Hz)) > 2 s^{-1} at 800 MHz) yields the following exchange parameters: (p_E, k_{ex}) = (7.98 ± 0.20 %, 98.0 ± 2.6 s^{-1}) for the ^{15}N [0013] TROSY-CPMG experiment and (8.89 ± 0.15 %, 89.6 ± 1.6 s^{-1}) for the ^{15}N ST-CW-CPMG experiment. Additionally, a favorable correlation is observed for the absolute values of chemical shift differences $|\Delta\varpi_{GE}|$ between ground and excited states in these two experiments (Fig. 6).

CPMG relaxation dispersion profiles were also recorded for an L99A variant of T4 lysozyme, L99A T4L [55], where the substitution of Ala for Leu generates a 150 Å^3 buried cavity in the C-terminal domain of the protein, leading to structural destabilization and consequently μs–ms timescale motions [56,57]. Comparative analyses have been performed using data recorded both with [0013]- and constant phase ^{15}N TROSY- and anti-TROSY-based CPMG experiments as well as with the ^{15}N ST-CW-CPMG sequence. As expected, the [0013]-set of experiments is superior to those based on constant phase pulses,

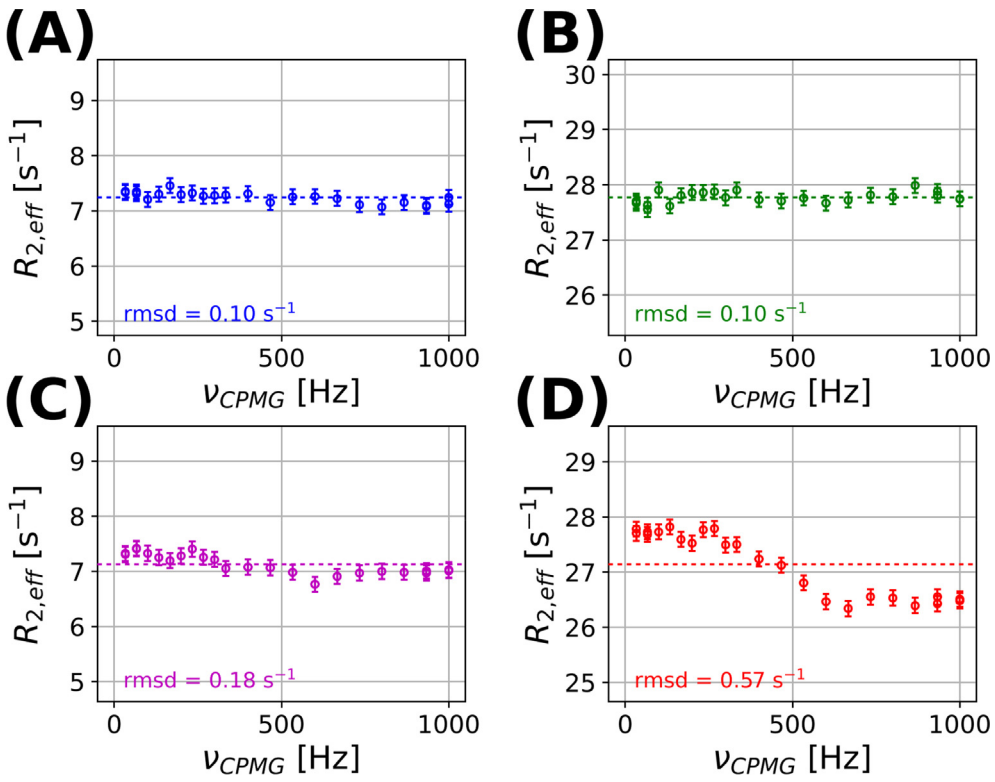

Fig. 5. Experimental results for K52 (^{15}N offset ~500 Hz) of protein L at 4 °C, 800 MHz, using the TROSY- (A) and anti-TROSY- (B) based ^{15}N CPMG experiments of Fig. 2. Similar TROSY (C) and anti-TROSY (D) data are presented using experiments with CPMG pulse trains of constant phase [18]. The RMSD of points of each curve to a best fit horizontal line (*dashes*) is indicated in each panel. The artifactual dispersion profiles in panels C and D can be well captured by numerical simulations performed with suitable parameters (Fig. 1, panels C and F, 10 % RF field inhomogeneity).

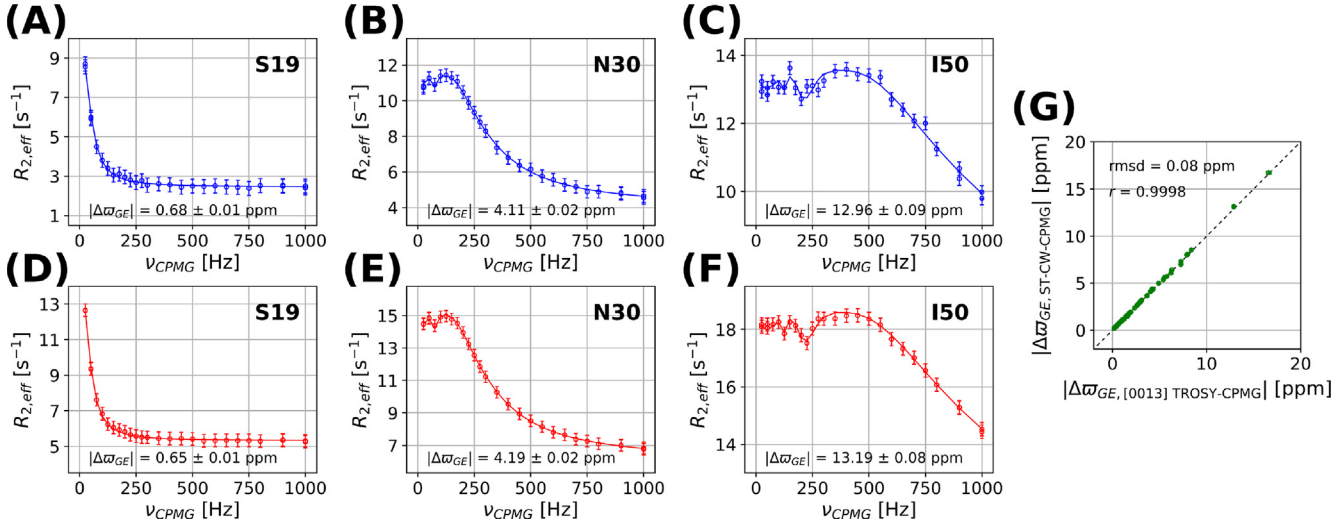

Fig. 6. ^{15}N TROSY CPMG relaxation dispersion profiles obtained with the experiment of Fig. 2 (panels A–C) and the ^{15}N ST-CW-CPMG scheme (panels D–F) for selective residues of G48A FynSH3, 25 °C, 800 MHz. Panel G shows the correlation between the chemical shift differences $|\Delta\omega_{GE}|$ obtained from the two experiments.

with smaller residual χ^2 values from fits of most residues, and this improvement is more pronounced in ^{15}N anti-TROSY-based CPMG experiments (Fig. 7). Notably, there is a significant difference in the sizes of the anti-TROSY dispersion profiles recorded with the different CPMG cycling schemes. This results from the fact that in the [0013]-version of the experiment R_1 contributions to $R_{2,eff}$ from off-resonance CPMG pulses are accounted for 'on the fly', while there is no compensation in the earlier experiments [18], Fig. 3G, 3H. This difference does not mean that robust exchange parameters can only be extracted using [0013]-versions of the experiment. Indeed, so long as the nuanced details of each pulse scheme are taken into account in fits of the data using a numerical approach such as *ChemEx* [44] accurate parameters can be obtained. For example, based on 56 residues which exhibit substantial CPMG relaxation dispersions (profiles with $\Delta R_{2,eff}$ (= $R_{2,eff}(\nu_{CPMG}$ = 33 Hz) − $R_{2,eff}(\nu_{CPMG}$ = 1000 Hz)) > 2 s^{-1} at 800 MHz), and fitting only the anti-TROSY data, (p_E, k_{ex}) = (3.38 ± 0.09 %, 1220 ± 48 s^{-1}) and (3.50 ± 0.25 %, 1159 ± 138 s^{-1}) result from analysis of profiles recorded with the schemes

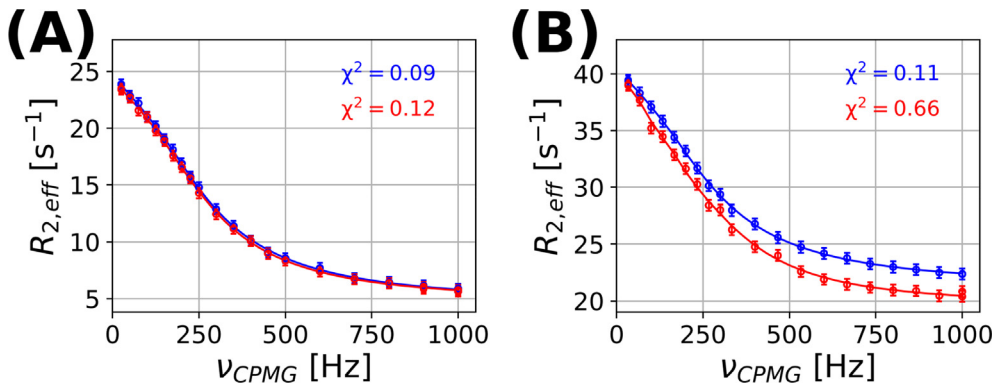

Fig. 7. Comparison of CPMG dispersion profiles for S136 (^{15}N offset ~400 Hz) of L99A T4L (25 °C, 800 MHz) recorded with the schemes of Fig. 2 (*blue*) and of Vallurupalli et al. (constant CPMG phase; *red*) [18]. Panels A and B show fits of the data for TROSY- (A) and anti-TROSY- (B) CPMG experiments to a model of two-site chemical exchange. The fitting residual χ^2 values are indicated in each panel, with the same color as the corresponding dispersion curve.

of Fig. 2 and from Vallurupalli et al. [18], respectively. We have also compared exchange parameters extracted from fits of profiles generated with the ^{15}N [0013] TROSY-CPMG experiment with those from a similar analysis of ^{15}N ST-CW-CPMG data. Values of (p_E, k_{ex}) = (3.53 ± 0.03 %, 1240 ± 8 s^{-1}) and (3.46 ± 0.03 %, 1234 ± 7 s^{-1}) are obtained from the two experiments, with a high correlation observed for the absolute value of chemical shift differences between spins in the ground and excited states (r = 0.997).

4. Concluding remarks

The importance of phase cycling is well understood in the design of modern pulse sequences, both for the removal of artifacts and for directing the flow of magnetization along desired coherence transfer pathways. Notably, although the need for minimizing artifacts of refocusing pulses in CPMG pulse trains is appreciated, there has been some [23–26,32,33,47], albeit comparatively less effort directed in the use of phase cycles in this area. Here, building on the [0013]-phase cycle proposed previously [32], we present a detailed calculation showing how such a scheme can be added into an existing set of TROSY and anti-TROSY CPMG experiments [18,37]. The resulting experiments, which also compensate properly for evolution during the CPMG pulses, and include an S^{3}E element [53] to select for either TROSY or anti-TROSY magnetization components at the start of the CPMG interval, show marked improvements in data quality relative to previous pulse sequences. It is anticipated that the proposed experiments will result in more robust exchange parameters, including RDC values obtained when both TROSY and anti-TROSY profiles are analyzed together [18].

CRediT authorship contribution statement

Yingxian Cui: Investigation, Formal analysis, Data curation. **Yangzhuoyue Jin:** Investigation, Formal analysis, Data curation. **Yu Hou:** Investigation, Resources. **Xiaoxu Han:** Investigation, Resources. **Haiyan Cao:** Investigation, Resources. **Lewis E. Kay:** Writing – review & editing, Writing – original draft, Supervision, Resources, Methodology, Investigation, Funding acquisition. **Tairan Yuwen:** Writing – review & editing, Writing – original draft, Validation, Supervision, Resources, Project administration, Methodology, Investigation, Funding acquisition, Formal analysis, Data curation, Conceptualization.

Data availability

Data will be made available on request. Example datasets are also available at the Mendeley Data Site (https://data.mendeley.com/datasets/4wzgyxzhpv).

Declaration of competing interest

The authors declare the following financial interests/personal relationships which may be considered as potential competing interests: L.E.K is an associate editor of this journal (JMR). If there are other authors, they declare that they have no known competing financial interests or personal relationships that could have appeared to influence the work reported in this paper.

Acknowledgements

This work was supported by the Beijing Natural Science Foundation in the form of a grant to T.Y. (Grant 7232251) and by grants from the Canadian Institutes of Health Research (Grant FDN-503573) and the Natural Sciences and Engineering Research Council of Canada (Grant 2015-04347) to L.E.K. We thank Dr. Pramodh Vallurupalli and Dr. Vitali Tugarinov for insightful discussion on pulse sequence design, and Dr. Guillaume Bouvignies for the assistance in data fitting with *ChemEx*. We are grateful to the NMR platform of State Key Laboratory of Natural and Biomimetic Drugs at Peking University for generously providing NMR spectrometer time.

Appendix A. Supplementary material

Supplementary material to this article can be found online at https://doi.org/10.1016/j.jmr.2024.107629.

References

[1] D.D. Boehr, D. McElheny, H.J. Dyson, P.E. Wright, The dynamic energy landscape of dihydrofolate reductase catalysis, Science 313 (2006) 1638–1642.
[2] K. Henzler-Wildman, D. Kern, Dynamic personalities of proteins, Nature 450 (2007) 964–972.
[3] T.R. Alderson, L.E. Kay, NMR spectroscopy captures the essential role of dynamics in regulating biomolecular function, Cell 184 (2021) 577–595.
[4] M. Karplus, J. Kuriyan, Molecular dynamics and protein function, Proc. Natl. Acad. Sci. U. S. A. 102 (2005) 6679–6685.
[5] N.L. Fawzi, J. Ying, R. Ghirlando, D.A. Torchia, G.M. Clore, Atomic-resolution dynamics on the surface of amyloid-β protofibrils probed by solution NMR, Nature 480 (2011) 268–272.
[6] A. Sekhar, J.A.O. Rumfeldt, H.R. Broom, C.M. Doyle, G. Bouvignies, E.M. Meiering, L.E. Kay, Thermal fluctuations of immature SOD1 lead to separate folding and misfolding pathways, Elife 4 (2015) e07296.
[7] P. Neudecker, P. Robustelli, A. Cavalli, P. Walsh, P. Lundström, A. Zarrine-Afsar, S. Sharpe, M. Vendruscolo, L.E. Kay, Structure of an intermediate state in protein folding and aggregation, Science 336 (2012) 362–366.
[8] I.R. Kleckner, M.P. Foster, An introduction to NMR-based approaches for measuring protein dynamics, Biochim. Biophys. Acta 2011 (1814) 942–968.
[9] A.G. Palmer, Chemical exchange in biomacromolecules: Past, present, and future, J. Magn. Reson. 241 (2014) 3–17.
[10] A.G. Palmer, C.D. Kroenke, J.P. Loria, Nuclear magnetic resonance methods for quantifying microsecond-to-millisecond motions in biological macromolecules, Methods Enzymol. 339 (2001) 204–238.

[11] D.M. Korzhnev, X. Salvatella, M. Vendruscolo, A.A. Di Nardo, A.R. Davidson, C.M. Dobson, L.E. Kay, Low-populated folding intermediates of Fyn SH3 characterized by relaxation dispersion NMR, Nature 430 (2004) 586–590.
[12] P. Vallurupalli, G. Bouvignies, L.E. Kay, Studying "invisible" excited protein states in slow exchange with a major state conformation, J. Am. Chem. Soc. 134 (2012) 8148–8161.
[13] P. Vallurupalli, A. Sekhar, T. Yuwen, L.E. Kay, Probing conformational dynamics in biomolecules via chemical exchange saturation transfer: a primer, J. Biomol. NMR 67 (2017) 243–271.
[14] A.G. Palmer, F. Massi, Characterization of the dynamics of biomacromolecules using rotating-frame spin relaxation NMR spectroscopy, Chem. Rev. 106 (2006) 1700–1719.
[15] T.I. Igumenova, A.G. Palmer, Off-resonance TROSY-selected $R_{1\rho}$ experiment with improved sensitivity for medium- and high-molecular-weight proteins, J. Am. Chem. Soc. 128 (2006) 8110–8111.
[16] N.J. Anthis, G.M. Clore, Visualizing transient dark states by NMR spectroscopy, Q. Rev. Biophys. 48 (2015) 35–116.
[17] A. Sekhar, L.E. Kay, An NMR view of protein dynamics in health and disease, Annu. Rev. Biophys. 48 (2019) 297–319.
[18] P. Vallurupalli, D.F. Hansen, E. Stollar, E. Meirovitch, L.E. Kay, Measurement of bond vector orientations in invisible excited states of proteins, Proc. Natl. Acad. Sci. U. S. A. 104 (2007) 18473–18477.
[19] D.F. Hansen, P. Vallurupalli, L.E. Kay, Measurement of methyl group motional parameters of invisible, excited protein states by NMR spectroscopy, J. Am. Chem. Soc. 131 (2009) 12745–12754.
[20] D. Long, G. Bouvignies, L.E. Kay, Measuring hydrogen exchange rates in invisible protein excited states, Proc. Natl. Acad. Sci. U. S. A. 111 (2014) 8820–8825.
[21] J.B. Stiller, R. Otten, D. Häussinger, P.S. Rieder, D.L. Theobald, D. Kern, Structure determination of high-energy states in a dynamic protein ensemble, Nature 603 (2022) 528–535.
[22] D. Xu, B. Li, J. Gao, Z. Liu, X. Niu, G. Nshogoza, J. Zhang, J. Wu, X. Su, W. He, R. Ma, D. Yang, K. Ruan, Ligand proton pseudocontact shifts determined from paramagnetic relaxation dispersion in the limit of NMR intermediate exchange, J. Phys. Chem. Lett. 9 (2018) 3361–3367.
[23] T. Yuwen, A. Sekhar, A.J. Baldwin, P. Vallurupalli, L.E. Kay, Measuring diffusion constants of invisible protein conformers by triple-quantum ^{1}H CPMG relaxation dispersion, Angew. Chem. Int. Ed. Engl. 57 (2018) 16777–16780.
[24] T. Yuwen, P. Vallurupalli, L.E. Kay, Enhancing the sensitivity of CPMG relaxation dispersion to conformational exchange processes by multiple-quantum spectroscopy, Angew. Chem. Int. Ed. Engl. 55 (2016) 11490–11494.
[25] T. Yuwen, R. Huang, P. Vallurupalli, L.E. Kay, A methyl-TROSY-based ^{1}H relaxation dispersion experiment for studies of conformational exchange in high molecular weight proteins, Angew. Chem. Int. Ed. Engl. 58 (2019) 6250–6254.
[26] V.Y. Orekhov, D.M. Korzhnev, L.E. Kay, Double- and zero-quantum NMR relaxation dispersion experiments sampling millisecond time scale dynamics in proteins, J. Am. Chem. Soc. 126 (2004) 1886–1891.
[27] M.D. Hürlimann, Carr–Purcell sequences with composite pulses, J. Magn. Reson. 152 (2001) 109–123.
[28] V.D.M. Koroleva, S. Mandal, Y. Song, M.D. Hürlimann, Broadband CPMG sequence with short composite refocusing pulses, J. Magn. Reson. 230 (2013) 64–75.
[29] M. Zweckstetter, T.A. Holak, An adiabatic multiple spin-echo pulse sequence: Removal of systematic errors due to pulse imperfections and off-resonance effects, J. Magn. Reson. 133 (1998) 134–147.
[30] T.W. Borneman, M.D. Hürlimann, D.G. Cory, Application of optimal control to CPMG refocusing pulse design, J. Magn. Reson. 207 (2010) 220–233.
[31] Y. Li, M. Rance, A.G. Palmer, Rotation operator propagators for time-varying radiofrequency pulses in NMR spectroscopy: Applications to shaped pulses and pulse trains, J. Magn. Reson. 248 (2014) 105–114.
[32] G.N.B. Yip, E.R.P. Zuiderweg, A phase cycle scheme that significantly suppresses offset-dependent artifacts in the R_2-CPMG ^{15}N relaxation experiment, J. Magn. Reson. 171 (2004) 25–36.
[33] B. Jiang, B. Yu, X. Zhang, M. Liu, D. Yang, A ^{15}N CPMG relaxation dispersion experiment more resistant to resonance offset and pulse imperfection, J. Magn. Reson. 257 (2015) 1–7.
[34] J.P. Loria, M. Rance, A.G. Palmer, A relaxation-compensated Carr–Purcell–Meiboom–Gill sequence for characterizing chemical exchange by NMR spectroscopy, J. Am. Chem. Soc. 121 (1999) 2331–2332.
[35] D.F. Hansen, P. Vallurupalli, L.E. Kay, An improved ^{15}N relaxation dispersion experiment for the measurement of millisecond time-scale dynamics in proteins, J. Phys. Chem. B 112 (2008) 5898–5904.
[36] K. Pervushin, R. Riek, G. Wider, K. Wüthrich, Attenuated T_2 relaxation by mutual cancellation of dipole–dipole coupling and chemical shift anisotropy indicates an avenue to NMR structures of very large biological macromolecules in solution, Proc. Natl. Acad. Sci. U. S. A. 94 (1997) 12366–12371.
[37] J.P. Loria, M. Rance, A.G. Palmer, A TROSY CPMG sequence for characterizing chemical exchange in large proteins, J. Biomol. NMR 15 (1999) 151–155.
[38] A. Mittermaier, L.E. Kay, χ_1 torsion angle dynamics in proteins from dipolar couplings, J. Am. Chem. Soc. 123 (2001) 6892–6903.
[39] G. Bouvignies, L.E. Kay, A 2D ^{13}C-CEST experiment for studying slowly exchanging protein systems using methyl probes: an application to protein folding, J. Biomol. NMR 53 (2012) 303–310.
[40] G. Bouvignies, P. Vallurupalli, L.E. Kay, Visualizing side chains of invisible protein conformers by solution NMR, J. Mol. Biol. 426 (2014) 763–774.
[41] G. Bouvignies, P. Vallurupalli, D.F. Hansen, B.E. Correia, O. Lange, A. Bah, R.M. Vernon, F.W. Dahlquist, D. Baker, L.E. Kay, Solution structure of a minor and transiently formed state of a T4 lysozyme mutant, Nature 477 (2011) 111–114.
[42] F.A.A. Mulder, N.R. Skrynnikov, B. Hon, F.W. Dahlquist, L.E. Kay, Measurement of slow (μs–ms) time scale dynamics in protein side chains by ^{15}N relaxation dispersion NMR spectroscopy: Application to Asn and Gln residues in a cavity mutant of T4 lysozyme, J. Am. Chem. Soc. 123 (2001) 967–975.
[43] F. Delaglio, S. Grzesiek, G.W. Vuister, G. Zhu, J. Pfeifer, A. Bax, NMRPipe: A multidimensional spectral processing system based on UNIX pipes, J. Biomol. NMR 6 (1995) 277–293.
[44] G. Bouvignies, ChemEx: NMR Chemical Exchange Analysis Tool, https://github.com/gbouvignies/ChemEx, GitHub (2023).
[45] P. Allard, M. Helgstrand, T. Härd, The complete homogeneous master equation for a heteronuclear two-spin system in the basis of Cartesian product operators, J. Magn. Reson. 134 (1998) 7–16.
[46] M. Helgstrand, T. Härd, P. Allard, Simulations of NMR pulse sequences during equilibrium and non-equilibrium chemical exchange, J. Biomol. NMR 18 (2000) 49–63.
[47] T. Yuwen, L.E. Kay, Revisiting $^{1}H^{N}$ CPMG relaxation dispersion experiments: a simple modification can eliminate large artifacts, J. Biomol. NMR 73 (2019) 641–650.
[48] T. Gullion, D.B. Baker, M.S. Conradi, New, compensated Carr–Purcell sequences, J. Magn. Reson. 89 (1990) 479–484.
[49] T. Yuwen, N.R. Skrynnikov, Proton-decoupled CPMG: A better experiment for measuring ^{15}N R_2 relaxation in disordered proteins, J. Magn. Reson. 241 (2014) 155–169.
[50] M.D. Sørensen, A. Meissner, O.W. Sørensen, Spin-state-selective coherence transfer via intermediate states of two-spin coherence in IS spin systems: Application to E. COSY-type measurement of J coupling constants, J. Biomol. NMR 10 (1997) 181–186.
[51] C.D. Kroenke, J.P. Loria, L.K. Lee, M. Rance, A.G. Palmer, Longitudinal and transverse ^{1}H–^{15}N dipolar/^{15}N chemical shift anisotropy relaxation interference: Unambiguous determination of rotational diffusion tensors and chemical exchange effects in biological macromolecules, J. Am. Chem. Soc. 120 (1998) 7905–7915.
[52] O.W. Sørensen, G.W. Eich, M.H. Levitt, G. Bodenhausen, R.R. Ernst, Product operator formalism for the description of NMR pulse experiments, Prog. Nucl. Magn. Reson. Spectrosc. 16 (1983) 163–192.
[53] A. Meissner, J.Ø. Duus, O.W. Sørensen, Spin-state-selective excitation. Application for E.COSY-type measurement of J_{HH} coupling constants, J. Magn. Reson. 128 (1997) 92–97.
[54] D.F. Hansen, H. Feng, Z. Zhou, Y. Bai, L.E. Kay, Selective characterization of microsecond motions in proteins by NMR relaxation, J. Am. Chem. Soc. 131 (2009) 16257–16265.
[55] A.E. Eriksson, W.A. Baase, J.A. Wozniak, B.W. Matthews, A cavity-containing mutant of T4 lysozyme is stabilized by buried benzene, Nature 355 (1992) 371–373.
[56] F.A.A. Mulder, A. Mittermaier, B. Hon, F.W. Dahlquist, L.E. Kay, Studying excited states of proteins by NMR spectroscopy, Nat. Struct. Biol. 8 (2001) 932–935.
[57] N.R. Skrynnikov, F.A.A. Mulder, B. Hon, F.W. Dahlquist, L.E. Kay, Probing slow time scale dynamics at methyl-containing side chains in proteins by relaxation dispersion NMR measurements: Application to methionine residues in a cavity mutant of T4 lysozyme, J. Am. Chem. Soc. 123 (2001) 4556–4566.
[58] L.E. Kay, P. Keifer, T. Saarinen, Pure absorption gradient enhanced heteronuclear single quantum correlation spectroscopy with improved sensitivity, J. Am. Chem. Soc. 114 (1992) 10663–10665.
[59] H. Geen, R. Freeman, Band-selective radiofrequency pulses, J. Magn. Reson. 93 (1991) 93–141.